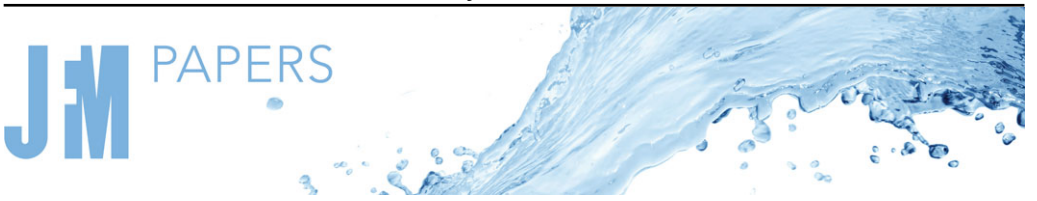
J. Fluid Mech. (2025), *vol.* 1009, A54, doi:10.1017/jfm.2025.267



Properties and asymptotics of water waves nonlinear interaction coefficient

Vladimir Geogjaev[1,2]

[1]Shirshov Institute of Oceanology of Russian Academy of Sciences, Nakhimovsky pr. 36, Moscow 117997, Russia

[2]Skolkovo Institute of Science and Technology, Bolshoy Boulevard 30, bld.1, Moscow 121205, Russia

Corresponding author: Vladimir Geogjaev, vvg@mail.geogjaev.ru

(Received 15 July 2024; revised 21 February 2025; accepted 26 February 2025)

The Hasselmann equation for the nonlinear interactions of deep-water gravity waves differs from other four-wave kinetic equations by the interaction coefficient. The explicit formula for this coefficient (e.g. Krasitskii, *J. Fluid. Mech.*, vol. 272, 1994, pp. 1–20; Zakharov, *Eur. J. Mech. B/Fluids,* vol. 18. issue 3, 1999, pp. 327–344) is of great complexity and leaves its properties obscured. We provide analytical results for the behaviour of the coefficient in different domains. The Phillips curve and discrete interaction approximation-like quadruplets are studied in detail. The coupling coefficient for the long–short wave interactions is calculated and found to be surprisingly small. This smallness greatly reduces the non-locality of the interactions.

Key words: turbulence theory, surface gravity waves, wave-structure interactions

1. Introduction

Gravity water waves are a significant and important example of dynamic systems. The Hamiltonian approach to their evolution (Zakharov 1968) has lead to the construction of the dynamic equation that describes the wave evolution. The wave steepness is used as a small parameter to expand the equation into the series of multi-wave interactions. The exclusion of non-resonant interactions with the use of a canonical transform of the dynamic variables yields the reduced Zakharov equation. The leading-order interactions for water waves are four-wave interactions. The interaction coefficient T for those interactions is the subject of the present paper.

The gravity water waves theory is the basis for the water waves modelling that has significant value in practical areas such as weather prediction and general climate applications. The complexity of four-wave interactions makes the existing wave models computationally expensive. The study of the interaction coefficient not only has a

© The Author(s), 2025. Published by Cambridge University Press.

https://doi.org/10.1017/jfm.2025.267 Published online by Cambridge University Press

theoretical value, but may help to improve the speed of the wave models. The efficiency may be improved by focusing on the interactions that transfer the main part of energy, and decreasing the calculation intensity for less significant interactions. Also, the approximations introduced in the present paper may provide a way to simplify the testing of model correctness.

The statistical description of the nonlinear interactions allows the derivation of the kinetic equation describing so-called wave turbulence. The kinetic equation includes interactions between sets of four waves (quadruplets) that are resonant in both space and time. The wave turbulence is a phenomenon of significant practical interest as well as a fundamental object for theoretical studies.

Both the kinetic equation and the reduced Zakharov equation have been extensively studied analytically and numerically (e.g. Komen, Hasselmann & Hasselmann 1984; Badulin *et al.* 2005; Annenkov & Shrira 2013; Zakharov *et al.* 2019). The multi-dimensional integration in these equations is a challenging problem for direct calculations. Various simplified, partial and surrogate methods were developed to cope with this difficulty. The geometric properties of interacting quadruplets and the behaviour of the coupling coefficient of those quadruplets are of great importance in dealing with these equations.

The resonant quadruplets that appear in the kinetic equation constitute a manifold in the space of quadruplets. The T coefficient may be constrained to this manifold. Here, we study this coefficient for the wave turbulence described by the kinetic equation. Our results are obtained for the quadruplets on the resonance surface. The behaviour of T in the more general case of the Zakharov equation is also of interest, but in the present paper we focus on the resonant manifold for the kinetic equation only. These results may be helpful in dealing with the Zakharov equation too, but that would require a substantial generalisation to expand them beyond the resonance surface.

The coupling coefficient determines the rate of the energy exchange between different parts of the wave spectrum. It was calculated in explicit form in Krasitskii (1994) and Zakharov (1999). An alternative, simpler form of the coefficient was obtained by Geogjaev & Zakharov (2017).

The formula for the coefficient (see (2.5) below) leaves the behaviour and properties of the coefficient obscured. The dependence of the coefficient on many variables (namely, four two-dimensional wave vectors) complicates the problem.

We restrict ourselves to the deep-water case, utilising the fact that the interacting coefficient for deep-water waves does not include a specific physical scale. Thus scaling can be used to eliminate one of the independent variables to simplify the formulae.

The coefficient T depends on four two-dimensional wave vectors (eight variables). The spatial (two-dimensional) and temporal resonant conditions for the kinetic equation allow for the elimination of three variables. The isotropy and scaling invariance enable us to eliminate two more variables. This allows us to introduce a 'normalised' T that depends on three variables only. These variables describe a three-dimensional manifold of resonant quadruplets. This manifold may be naturally divided into domains with different behaviours of T that are parametrised by two variables. This simplification allows us to derive some approximate formulae for T.

The complexity of the quadruplet nonlinear interaction mechanism and the needs of operational wave forecasting have led to the development of simplified methods of calculation of the collision integral. The quadruplets of interacting wave vectors, though originating from the same resonant condition, are quite different in properties and in their effect on the spectrum evolution. If calculations are restricted to some part of the

https://doi.org/10.1017/jfm.2025.267 Published online by Cambridge University Press

quadruplet space, then the quadruplets may be simplified while preserving the general properties of the nonlinear energy transfer.

The discrete interaction approximation (DIA) method proposed by Hasselmann *et al.* (1985) is a well-known simplified method of the nonlinear transfer calculation. Its main idea is to use of one of the quadruplets to represent all nonlinear interactions. The coupling coefficient for this single quadruplet is determined empirically. The DIA method retains the quadruplet properties of interactions and does not break the conservation laws.

The result of such a simplification was surprisingly good. The utility of the DIA method was confirmed in, for example, Komen *et al.* (1994), Tolman (2004), Benoit (2005), Alves *et al.* (2007, § 2.2) and Gagnaire-Renou, Benoit & Badulin (2011). Below, in § 4.1, we reveal some reasons and justifications for DIA viability. The main reason is that a large part of the manifold of quadruplets is populated by quadruplets similar to the DIA one, and the DIA quadruplet may represent them with reasonable accuracy.

The DIA quadruplet depends on a parameter λ, the choice of which is somewhat arbitrary. The multiple DIA method (Hashimoto & Kawaguchi 2001) improves DIA by using multiple DIA-like quadruplets.

Another kind of simplification is the restriction of the interactions to the energy transfer between four nearly equal wave vectors. This is valid for the case of narrow spectrum but, with caveats, may still be applicable to more general spectra. This approach was developed in Dungey & Hui (1979); we discuss it briefly in § 4.2.

The numerical solving of the general dynamic equation is more challenging. For an approach to its numerical solving, see Annenkov & Shrira (2001).

The article is organised in the following way. Section 3 briefly describes the properties of resonant quadruplets and introduce the variables for their representation. Section 4 is a description of various classes of quadruplets: § 4.1 is devoted to interactions with the central part of the quadruplet manifold (DIA-like quadruplets), which plays the most significant role in energy transfer; § 4.2 describes the central part of the quadruplet manifold itself (where all the wave vectors are nearly equal). Subsection 4.3 describe the asymptotic behaviour of T for the interactions between long and short waves. These interactions are strongly non-local, but the effect of the non-locality is greatly diminished by the smallness of T. The calculation of this asymptotic is included as Appendix B. Subsection 4.4 describes the asymptotic form of T for interactions between waves with wave vectors of close lengths but with different angles.

2. The Hasselmann equation

The Hasselmann equation (Hasselmann 1962) is the kinetic equation for gravity water waves. It reads

$$\begin{aligned}\frac{\mathrm{d}N_{\boldsymbol{k}}}{\mathrm{d}t} = \pi g^2 \int\limits_{\boldsymbol{k}_2,\boldsymbol{k}_3,\boldsymbol{k}_4} \left(T_{\boldsymbol{k}\boldsymbol{k}_2\boldsymbol{k}_3\boldsymbol{k}_4}\right)^2 \\ \times \left(N_{\boldsymbol{k}_2}N_{\boldsymbol{k}_3}N_{\boldsymbol{k}_4} + N_{\boldsymbol{k}}N_{\boldsymbol{k}_3}N_{\boldsymbol{k}_4} - N_{\boldsymbol{k}}N_{\boldsymbol{k}_2}N_{\boldsymbol{k}_4} - N_{\boldsymbol{k}}N_{\boldsymbol{k}_2}N_{\boldsymbol{k}_3}\right) \\ \times \delta(\boldsymbol{k}+\boldsymbol{k}_2-\boldsymbol{k}_3-\boldsymbol{k}_4)\,\delta(\omega+\omega_2-\omega_3-\omega_4)\,\mathrm{d}\boldsymbol{k}_2\,\mathrm{d}\boldsymbol{k}_3\,\mathrm{d}\boldsymbol{k}_4. \end{aligned} \tag{2.1}$$

Here, $N(\boldsymbol{k})$ is the wave action spectrum. It is connected to the energy spectrum $\varepsilon(\boldsymbol{k})$ by the relation $N = \varepsilon/\omega$, where ω is the wave frequency.

Equation (2.1) includes two δ-functions that define the resonant conditions:

https://doi.org/10.1017/jfm.2025.267 Published online by Cambridge University Press

$$\boldsymbol{k}_1 + \boldsymbol{k}_2 = \boldsymbol{k}_3 + \boldsymbol{k}_4, \tag{2.2}$$

$$\omega_1 + \omega_2 = \omega_3 + \omega_4. \tag{2.3}$$

Only waves satisfying these conditions may exchange their energy through nonlinear interactions.

Wave frequency $\omega(\boldsymbol{k})$ obeys the dispersion relation. In the present paper we deal with deep-water surface waves for which

$$\omega = \sqrt{gk}, \tag{2.4}$$

where g is the gravity acceleration. Other waves, such as gravity-capillary waves or finite-depth waves, have extra dimensional parameters in their dispersion relation that would prevent the use of scaling.

The wave interaction intensity is determined by the coupling coefficient T. This paper focuses on the investigation of its properties.

The coefficient T first found in Hasselmann (1962) was calculated explicitly in Zakharov & Filonenko (1966) and Zakharov (1968). It was derived in Krasitskii (1994), with the account of canonical transformations that ensured the preservation of the Hamiltonian structure and the conservation of energy. In the review article by Zakharov (1999), T was written as

$$\begin{aligned}
T_{\boldsymbol{k}_1\boldsymbol{k}_2\boldsymbol{k}_3\boldsymbol{k}_4} = -\frac{1}{4(k_1k_2k_3k_4)^{1/4}} \Big\{ & -12k_1k_2k_3k_4 \\
& - 2(\omega_1+\omega_2)^2\left[\omega_3\omega_4\left(\boldsymbol{k}_1\boldsymbol{k}_2 - k_1k_2\right) + \omega_1\omega_2\left(\boldsymbol{k}_3\boldsymbol{k}_4 - k_3k_4\right)\right] \\
& - 2(\omega_1-\omega_3)^2\left[\omega_2\omega_4\left(\boldsymbol{k}_1\boldsymbol{k}_3 + k_1k_3\right) + \omega_1\omega_3\left(\boldsymbol{k}_2\boldsymbol{k}_4 + k_2k_4\right)\right] \\
& - 2(\omega_1-\omega_4)^2\left[\omega_2\omega_3\left(\boldsymbol{k}_1\boldsymbol{k}_4 + k_1k_4\right) + \omega_1\omega_4\left(\boldsymbol{k}_2\boldsymbol{k}_3 + k_2k_3\right)\right] \\
& + (\boldsymbol{k}_1\boldsymbol{k}_2 + k_1k_2)(\boldsymbol{k}_3\boldsymbol{k}_4 + k_3k_4) + (-\boldsymbol{k}_1\boldsymbol{k}_3 + k_1k_3)(-\boldsymbol{k}_2\boldsymbol{k}_4 + k_2k_4) \\
& + (-\boldsymbol{k}_1\boldsymbol{k}_4 + k_1k_4)(-\boldsymbol{k}_2\boldsymbol{k}_3 + k_2k_3) \\
& + 4(\omega_1+\omega_2)^2\frac{(\boldsymbol{k}_1\boldsymbol{k}_2 - k_1k_2)(\boldsymbol{k}_3\boldsymbol{k}_4 - k_3k_4)}{k_{1+2} - (\omega_1+\omega_2)^2} \\
& + 4(\omega_1-\omega_3)^2\frac{(\boldsymbol{k}_1\boldsymbol{k}_3 + k_1k_3)(\boldsymbol{k}_2\boldsymbol{k}_4 + k_2k_4)}{k_{1-3} - (\omega_1-\omega_3)^2} \\
& + 4(\omega_1-\omega_4)^2\frac{(\boldsymbol{k}_1\boldsymbol{k}_4 + k_1k_4)(\boldsymbol{k}_2\boldsymbol{k}_3 + k_2k_3)}{k_{2-3} - (\omega_1-\omega_4)^2} \Big\}.
\end{aligned} \tag{2.5}$$

Here, $k_{1+2} = |\boldsymbol{k}_1 + \boldsymbol{k}_2|$, $k_{1-3} = |\boldsymbol{k}_1 - \boldsymbol{k}_3|$, $k_{2-3} = |\boldsymbol{k}_2 - \boldsymbol{k}_3|$, $k_i = |\boldsymbol{k}_i|$, $\omega_i = \sqrt{k_i}$. We have set $g = 1$ to simplify the formulae. The apparent asymmetries in this formula may be eliminated with the use of the resonant conditions (2.3) and (2.2).

Other expressions for T were introduced in Webb (1978) and Lavrenov (2003) (for an overview, see Badulin *et al.* 2005).

It should be noted that different normalisations of T are currently in use. The normalisation that we have chosen simplifies the formulae and is convenient for the plotting. Equation (2.1) is written in the form that is compatible with (2.5).

In present paper, we deal with the coupling coefficient on a resonant surface (defined by (2.2) and (2.3)) only. We mention that in the general case of the Zakharov equation, the T coefficient allows some freedom due to the choice of canonical transformation (Krasitskii 1994). Formula (2.5) is still valid (with a proper symmetrisation).

https://doi.org/10.1017/jfm.2025.267 Published online by Cambridge University Press

3. Properties of quadruplets

3.1. *General description of quadruplets*

We define a quadruplet as four wave vectors $\boldsymbol{k}_1$, $\boldsymbol{k}_2$, $\boldsymbol{k}_3$, $\boldsymbol{k}_4$ satisfying the resonant conditions (2.2) and (2.3). These quadruplets constitute a five-dimensional manifold. We perform a normalisation of quadruplets with respect to direction and scale to introduce a three-dimensional manifold of normalised quadruplets.

The kinetic equation (2.1) is isotropic, so the properties of a quadruplet must not depend on its orientation. We fix the orientation by fixing the direction of the $\boldsymbol{k}_{1+2}$ vector. All the angles will be measured with respect to this vector.

The coefficient T with dispersion relation (2.4) permits the scaling

$$T(a\boldsymbol{k}_1, a\boldsymbol{k}_2, a\boldsymbol{k}_3, a\boldsymbol{k}_4) = a^3\, T(\boldsymbol{k}_1, \boldsymbol{k}_2, \boldsymbol{k}_3, \boldsymbol{k}_4). \tag{3.1}$$

We will use the 'base vector' $\boldsymbol{k}_B = \boldsymbol{k}_{1+2}/2$ as the scale base. All the vectors will be normalised to k_B, while T will be normalised to k_B^3. This T normalisation is convenient everywhere except in the region where k_{1+2} is small ('angular quadruplets'; see § 4.4). In that region, we have to use $(k_1k_2k_3k_4)^{3/4}$ as the normalisation for T.

The difference between the two normalisations does not affect the general behaviour of T. The notable exceptions are the quadruplets with small k_{1+2} mentioned above, and the long–short interactions (see § 4.3).

It is well known (Longuet-Higgins 1976) that for equal vectors $\boldsymbol{k}_1 = \boldsymbol{k}_2 = \boldsymbol{k}_3 = \boldsymbol{k}_4 = \boldsymbol{k}_B$, we have

$$k_B^{-3}\, T(\boldsymbol{k}, \boldsymbol{k}, \boldsymbol{k}, \boldsymbol{k}) = 2. \tag{3.2}$$

An appropriate choice of normalisation allows us to find that for opposite vectors $\boldsymbol{k}_1 = -\boldsymbol{k}_2$, $\boldsymbol{k}_3 = -\boldsymbol{k}_4$, we have $k_1 = k_2 = k_3 = k_4 = k$ and

$$k^{-3}\, T(\boldsymbol{k}, -\boldsymbol{k}, \boldsymbol{k}, -\boldsymbol{k}) = -2. \tag{3.3}$$

We will suggest below that these values are local extrema. Numerical calculations show that the normalised T is globally bounded by these values:

$$-2 \leqslant \frac{T(\boldsymbol{k}_1, \boldsymbol{k}_2, \boldsymbol{k}_3, \boldsymbol{k}_4)}{(k_1k_2k_3k_4)^{3/4}} \leqslant 2. \tag{3.4}$$

The T coefficient is invariant with respect to several permutations of vectors. These are the $\boldsymbol{k}_1 \leftrightarrow \boldsymbol{k}_2$ permutation, the $\boldsymbol{k}_3 \leftrightarrow \boldsymbol{k}_4$ permutation, and also the double permutation $\boldsymbol{k}_1 \leftrightarrow \boldsymbol{k}_3$, $\boldsymbol{k}_2 \leftrightarrow \boldsymbol{k}_4$. This symmetry allows us to deal with only part of the quadruplet space. In particular, it is convenient to set

$$k_1 \leqslant k_2, \quad k_3 \leqslant k_4. \tag{3.5}$$

Some notable special cases may be mentioned. First, there is the case of pairwise coinciding vectors $\boldsymbol{k}_1 = \boldsymbol{k}_3$, $\boldsymbol{k}_2 = \boldsymbol{k}_4$ studied in Lavrova (1983). Such quadruplets do not transfer energy, for geometrical reasons, but have non-trivial T. Then there is the one-dimensional case when all the vectors are collinear, studied in Dyachenko *et al.* (2017). This case has two variants. First, the collinear vectors may be coinciding pairwise. Alternatively, three vectors may be of the same direction, with the fouth one of opposite direction. It is shown in Dyachenko & Zakharov (1994) and Dyachenko *et al.* (2017) that for such quadruplets, $T = 0$. Therefore, there is no four-wave interaction in the one-dimensional case. Nevertheless, this case is interesting for the study of nearly-collinear wave packets.

https://doi.org/10.1017/jfm.2025.267 Published online by Cambridge University Press

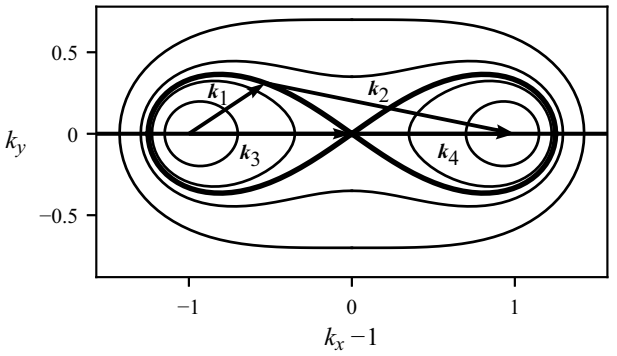


Figure 1. The 'Phllips eight' curve (thick line) and some other lines of $s = \text{const}$ (thin lines). Also shown is the DIA quadruplet ($s = 1$, $\lambda_1 = 0.25$, $\lambda_3 = 0$). k_x and k_y are the x and y coordinates of k_1 and k_3 vectors.

3.2. *Coordinates*

Fixing the normalisation and the direction leaves us with three coordinates of a quadruplet to deal with. Let us discuss the choice of these coordinates.

The coordinate that is convenient and significant in the classification of quadruplets is the 'modulus' s defined as

$$\omega_1 + \omega_2 = \omega_3 + \omega_4 = 2s\sqrt{gk_B}. \tag{3.6}$$

The modulus s is bounded by

$$\frac{\sqrt{2}}{2} < s < +\infty. \tag{3.7}$$

For the long–short interactions, $s = (\sqrt{2}/2)(1 + r)$, $r \ll 1$.

A significant case is $s = 1$; see § 4.1.

Large values of s correspond to the interactions between the vectors of close lengths but different directions.

The conditions

$$\begin{aligned} &\omega_1 + \omega_2 = 2s\sqrt{gk_B}, \\ &\boldsymbol{k}_1 + \boldsymbol{k}_2 = 2\boldsymbol{k}_B \end{aligned} \tag{3.8}$$

define a curve at the $\boldsymbol{k}$ plane for any s (figure 1 shows some such curves). Any two points of this curve define a quadruplet: $\boldsymbol{k}_1$ and $\boldsymbol{k}_2$ are defined by one point, and $\boldsymbol{k}_3$ and $\boldsymbol{k}_4$ by the other one. The quadruplet symmetry allows us to choose both these points on the left-hand side of the curve.

The Zakharov equation covers not only the resonant surface but the area outside it as well. The non-resonant quadruplets there may be described with two separate moduli defined by $(\omega_1 + \omega_2)/2$ and $(\omega_3 + \omega_4)/2$ (both equal to s on the resonant surface). Some approximations introduced here should be valid in the vicinity of the resonant surface, but these constructions are beyond the scope of the present paper. See Dyachenko *et al.* (2017) for some simplifications of T for the Zakharov equation.

We will use the parameter s for the classification of quadruplets. The remaining two coordinates are less significant. The simplest choice for them would be the angles θ_1 and θ_3 (which are measured between two smaller vectors and $\boldsymbol{k}_B$). Another option is to use λ_1 and λ_3 (the numbering correspond to the numbering of wave vectors) such that

https://doi.org/10.1017/jfm.2025.267 Published online by Cambridge University Press

$$\omega_1 = (1-\lambda_1)\sqrt{gk_B}, \quad \omega_2 = (1+\lambda_1)\sqrt{gk_B},$$
$$\omega_3 = (1-\lambda_3)\sqrt{gk_B}, \quad \omega_4 = (1+\lambda_3)\sqrt{gk_B}. \tag{3.9}$$

The advantage of $\lambda_{1,3}$ coordinates lies in the fact that all the parameters of quadruplet vectors may be derived from them using elementary functions only. Their drawback is the singularity at the horizontal axis. They are also double-valued.

Finally, we note that other parametrisations of the resonance manifold are possible. Moreover, the base vector may be chosen in other ways (e.g. one may use $\boldsymbol{k}_{1-3}$). We try to minimise the explicit use of our coordinates. Therefore, all the final formulae are written here in terms of the $\boldsymbol{k}$ vectors and without the use of the normalisation.

4. Quadruplet classes

4.1. *DIA-like quadruplets*

One of the first methods of simplification of the four-wave interaction pattern was suggested by Phillips (1960). He considered the resonance between a main wave taken twice, and two other waves. This corresponds to $\boldsymbol{k}_3 = \boldsymbol{k}_4$. In this case, the endpoints of the $\boldsymbol{k}_1$ and $\boldsymbol{k}_2$ vectors lie on the curve that is known as the 'Phillips eight' (figure 1).

The DIA method proposed by Hasselmann *et al.* (1985) uses only one symmetric pair of quadruplets. Historically, this was the first (though severely simplified) representation of (2.1) in quadruplet form. The DIA quadruplet is

$$\omega_1 = (1-\lambda)\omega_B, \quad \omega_2 = (1+\lambda)\omega_B, \quad \omega_3 = \omega_4 = \omega_B, \tag{4.1}$$

with $\lambda = 0.25$. This quadruplet is shown in figure 1.

The Phillips eight curve is indeed of great importance. Its central part is a geometric singularity. The large area around the singularity is populated by similar kinds of vector pairs. Vector pairs in the vicinity of the singularity ($\boldsymbol{k}_1 \approx \boldsymbol{k}_2 \approx \mathbf{1}$) are composed of two nearly equal vectors. If one substitutes such a pair by the two equal vectors (represented by the centre of the curve), then the resulting changes of the two vectors are small and anticollinear. The changes in N_i in (2.1) resulting from such a substitution compensate each other to first order due to the anticollinearity. This means that all the points near the centre may be substituted by the central point without a significant loss of precision. Such a substitution requires a shift of the other point of the quadruplet, but this shift is small for the points that are away from the centre because the curves of constant s converge there. This is why the DIA quadruplet may adequately represent a whole family of similar quadruplets. This explains the viability of the DIA method.

While the DIA-like quadruplets account for a significant part of the wave interactions, they do not represent the entire variety of interactions. Notably missing from the DIA method are interactions between waves of different angles (which play a role in the transfer of energy from the main peak of wind waves to the waves travelling sideways or against the wind). Also, the DIA method seriously limits the long–short waves interaction range.

The above considerations justify a dedicated study of the Phillips curve. In terms of the coordinates introduced above, this curve is defined by $s = 1$.

We introduce a class of DIA-like quadruplets defined by (4.1) with arbitrary λ. (For $s = 1$ we have $-1/2 \leqslant \lambda \leqslant 1/2$). The coefficient T for this case may be calculated explicitly as

$$T_{\boldsymbol{k}_1\boldsymbol{k}_2\boldsymbol{k}_B\boldsymbol{k}_B} = \frac{k_B^3}{2\sqrt{1-\lambda^2}}\left(2+\lambda^2\right)^2\left(1-4\lambda^2\right)\left(1-\frac{2}{3}\left(|\lambda|\sqrt{6+\lambda^2}+\lambda^2\right)\right). \tag{4.2}$$

This function is shown on figure 2 as the top line.

https://doi.org/10.1017/jfm.2025.267 Published online by Cambridge University Press

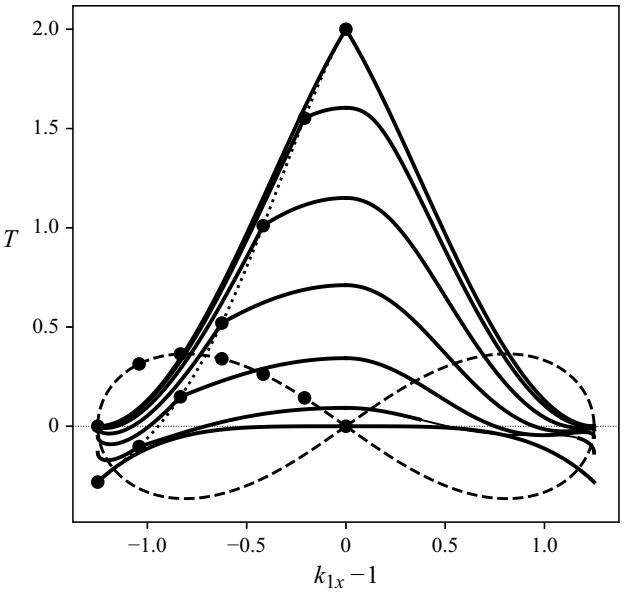


Figure 2. The T/k_B^3 coefficient graphs for the Phillips curve quadruplets. The quadruplets are specified by two points at the curve. One of them is fixed for each of the T curves (and chosen at the left-hand side of the Phillips curve), while the other moves at the top part of the 'eight' curve. The fixed point is marked both on the Phillips curve and in the corresponding T graph (at the same abscissa). The abscissa of the moving point is used as the T graph independent coordinate. The marks on the T graphs correspond to the quadruplets with coinciding vector pairs, which allows us to draw the graph of $T_{\boldsymbol{k}_1\boldsymbol{k}_2\boldsymbol{k}_1\boldsymbol{k}_2}$ through these marks (dotted line).

In particular, for the DIA quadruplet with $\lambda = 0.25$,

$$T_{DIA} \approx 0.903\, k_B^3. \tag{4.3}$$

At the sides of the Phillips curve, (4.2) is small. Let us take the θ_1 such that $\pi - \theta_1 \ll 1$ (which corresponds to the left-hand side of the curve). Then $\lambda \approx (1/2) - (\pi - \theta_1)^2/36$ and

$$T_{\boldsymbol{k}_1\boldsymbol{k}_2\boldsymbol{k}_B\boldsymbol{k}_B} \approx \frac{\sqrt{3}}{80}\, k_B^3\, (\pi - \theta_1)^4. \tag{4.4}$$

This implies that the interaction between the side and central part of the curve is small. The dynamically significant part of the curve is the central 'cross'. It may be defined approximately by $|\lambda| < 0.42$. (We take here the λ for $\theta_1 = \pi/2$, for this value $T \approx 0.14$.)

Now we explore arbitrary λ_1 and λ_3 (while still keeping $s = 1$). Figure 2 shows a set of graphs of T/k_B^3 for different λ_3 values. For clarity, the graph also shows the Phillips curve (dashed line). The abscissa axis represents $k_{1x} - 1$ (k_{1x} being the x-component of $\boldsymbol{k}_1$). This coordinate is used for both the Phillips curve and the T graphs; the corresponding λ_1 may be determined from k_{1x} as $k_{1x} - 1 = -2(\lambda_1 + \lambda_1^3)$. The set of fixed λ_3 points for the graphs is shown as dots on the Phillips curve. The points with $\lambda_1 = \lambda_3$ are marked on the graphs; these points constitute the $T_{\boldsymbol{k}_1\boldsymbol{k}_2\boldsymbol{k}_1\boldsymbol{k}_2}$ graph that is also shown (dotted line).

We also present a two-dimensional graph of T in figure 3. Obviously, this graph cannot represent the whole three-dimensional space of quadruplets, but it is useful for understanding of the general behaviour of T. The xy plane of this graph represents the points that define the $\boldsymbol{k}_1$ and $\boldsymbol{k}_2$ vectors; corresponding lines of s are also shown. The figure shows the T graph for the quadruplet defined by these $\boldsymbol{k}_1$, $\boldsymbol{k}_2$, while the $\boldsymbol{k}_3$, $\boldsymbol{k}_4$ are

https://doi.org/10.1017/jfm.2025.267 Published online by Cambridge University Press

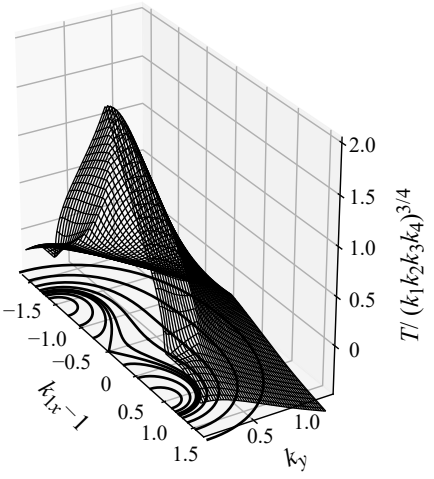


Figure 3. A two-dimensional cross-section of the $T/(k_1k_2k_3k_4)^{3/4}$ graph. To make this cross-section from the three-dimensional quadruplet space, one of the quadruplet points was chosen at the x axis for $s < 1$, or at the y axis for $s > 1$. The other point is used as the independent coordinate.

chosen as follows. For $s < 1$, the point representing $\boldsymbol{k}_3$ and $\boldsymbol{k}_4$ is chosen at the x axis such that $\boldsymbol{k}_3$ and $\boldsymbol{k}_B$ are collinear. For $s > 1$, such a point does not exist, and we use a central point such that $\boldsymbol{k}_{3y} = 1$. Such a choice yields $\boldsymbol{k}_3$ and $\boldsymbol{k}_4$ close to $\boldsymbol{k}_B$ whenever possible. The vertical axis represents $T/(k_1k_2k_3k_4)^{3/4}$. Such a normalisation is chosen for the graph to be finite.

The graph in figure 3 shows that T is large at the central zone. It crosses zero somewhere at a larger s, then continues to decrease up to the value -2 (beyond the graph boundary). Also note that at the ends of the Phillips curve, T is small (it is exactly zero at the adjacent part of the abscissa axis).

4.2. *Central quadruplets*

The central part of the quadruplet manifold (where all four vectors are nearly equal) is of particular interest. While most of the quadruplets describe non-local interactions, these central quadruplets are an example of the local interaction. They were studied before in Longuet-Higgins (1976) and Dungey & Hui (1979), where the expansion at the central point of the Phillips curve was used to construct an approximate diffusion-like method of calculation of the energy transfer. This approach results in the Dysthe equation, which is a generalisation of the nonlinear Schrödinger equation (Dysthe 1979).

The central quadruplets provide an interesting insight into the mechanism of energy transfer. Nevertheless, their transfer rate is weakened for geometrical reasons (the nearly equal vectors result in smaller difference in (2.1)). The DIA-like quadruplets described above still benefit from the large T and from the considerable width of the central area, but they also connect different parts of the spectrum (the length ratio between 'long' and 'short' vectors in the DIA quadruplet (4.1) is 2.78). For these reasons, they provide a large part of the energy transfer.

The central area includes many quadruplets and has a large (actually, maximum) T. In this domain,

$$\boldsymbol{k}_1 = \boldsymbol{k}_B - \varkappa_1, \quad \boldsymbol{k}_2 = \boldsymbol{k}_B + \varkappa_1, \quad \boldsymbol{k}_3 = \boldsymbol{k}_B - \varkappa_3, \quad \boldsymbol{k}_4 = \boldsymbol{k}_B + \varkappa_3, \tag{4.5}$$

https://doi.org/10.1017/jfm.2025.267 Published online by Cambridge University Press

where $\varkappa_1$ and $\varkappa_3$ are small parameters:

$$\varkappa_1 \ll k_B, \quad \varkappa_3 \ll k_B. \tag{4.6}$$

Then T is

$$T = 2k_B^3 \left\{ 1 - \frac{(\varkappa_{1x} - \varkappa_{3x})^2}{2\sqrt{(\varkappa_{1x} - \varkappa_{3x})^2 + (\varkappa_{1y} - \varkappa_{3y})^2}} - \frac{(\varkappa_{1x} + \varkappa_{3x})^2}{2\sqrt{(\varkappa_{1x} + \varkappa_{3x})^2 + (\varkappa_{1y} + \varkappa_{3y})^2}} + o(\varkappa) \right\}. \tag{4.7}$$

One can see from (4.7) that the first-order correction to T is negative except for $\varkappa_{1x} = \varkappa_{3x} = 0$. One more order is required to deal with the latter case. The second-order correction is also negative, which proves that $T_{\boldsymbol{kkkk}}$ is indeed the maximum. The details of the calculation are given in Appendix A.

We may restrict ourselves to the $s = 1$ curve. In this area, the curve is defined by

$$\varkappa_{1y} = \pm\frac{\sqrt{2}}{2}\varkappa_{1x}, \quad \varkappa_{3y} = \pm\frac{\sqrt{2}}{2}\varkappa_{3x}. \tag{4.8}$$

A quadruplet is defined by two points on this curve. If they are on the same branch of (4.8), then the expression (4.7) can be simplified:

$$T = 2k_B^3 \left\{ 1 - \frac{2\sqrt{6}}{3}\lambda_1 + o(\lambda) \right\}. \tag{4.9}$$

Here, we have set $|\lambda_1| > |\lambda_3|$. The result is independent of λ_3.

4.3. *Long–short interactions*

Equation (2.1) is non-local. It includes interactions between waves with different $\boldsymbol{k}$ that are not nesesserily close to each other. The most drastic case of non-locality is the long–short interaction. While most quadruplets are composed of vectors of comparable lengths, long–short interaction quadruplets may include vectors with an arbitrarily large length ratio.

We show that the interaction coefficient for the long–short interactions is surprisingly small. In the calculation of the coefficient, the two higher orders of the expansion turn out to be zero. The underlying reason for this is still unknown. This smallness significantly reduces the non-locality of the kinetic equation, and increases the role of energy and wavenumber cascading.

Figure 4 shows a typical long–short interaction quadruplet. Such quadruplets include two nearly equal long vectors $\boldsymbol{k}_2$, $\boldsymbol{k}_4$, and two short vectors $\boldsymbol{k}_1$, $\boldsymbol{k}_3$ that are approximately equal in length but have arbitrary directions.

We will use a small parameter r defined by

$$\omega_1 + \omega_2 = \omega_3 + \omega_4 = (1 + r)\sqrt{k_{1+2}}. \tag{4.10}$$

We have

$$k_2 \approx k_4 \approx k_{1+2}, \quad k_1 \approx k_3 \approx r^2 k_{1+2}. \tag{4.11}$$

The other two independent variables are θ_1 (the angle between $\boldsymbol{k}_1$ and $\boldsymbol{k}_{1+2}$) and θ_3 (the angle between $\boldsymbol{k}_3$ and $\boldsymbol{k}_{1+2}$).

https://doi.org/10.1017/jfm.2025.267 Published online by Cambridge University Press

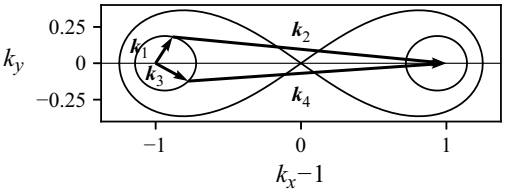


Figure 4. An example of a long–short quadruplet. Also shown are the Phillips curve and the $s = \text{const}$ curve for this quadruplet.

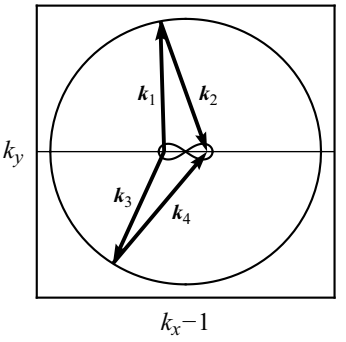


Figure 5. An example of an angular quadruplet. Also shown are the Phillips curve and the $s = \text{const}$ curve for this quadruplet.

Extremely complicated calculations (included here as Appendix B) yield the following result:

$$T = \frac{r^4 k_{1+2}^3}{2} \left(\cos\theta_1 + \cos\theta_3\right) \left(1 + \cos(\theta_1 - \theta_3)\right) + o\left(r^4\right). \tag{4.12}$$

The expansion of T by the small parameter r has a very surprising property: two higher orders of the expansion are zeros.

It may be that to some extent, the long–short interaction quadruplets border the quadruplets at the vicinity of the Phillips curve.

4.4. *Angular quadruplets*

A significant and distinct class of the quadruplets includes ones describing the interaction between the waves of close frequencies travelling in different directions. Their characteristic property is a small $\boldsymbol{k}_{1+2}$ vector. We propose to call them 'angular quadruplets'. An example of such a quadruplet is shown in figure 5.

For these quadruplets, we have

$$\boldsymbol{k}_2 \approx -\boldsymbol{k}_1, \quad \boldsymbol{k}_4 \approx -\boldsymbol{k}_3, \tag{4.13}$$

which results in

$$k_1 \approx k_2 \approx k_3 \approx k_4 \gg k_{1+2}. \tag{4.14}$$

Let k be the length of (approximately equal) vectors of an angular quadruplet. Then T becomes

$$T \approx -\frac{k^3}{2}\left(3 + \cos^2\theta_{1-3}\right), \tag{4.15}$$

where θ_{1-3} is the angle between $\boldsymbol{k}_1$ and $\boldsymbol{k}_3$ or between $\boldsymbol{k}_2$ and $\boldsymbol{k}_4$.

https://doi.org/10.1017/jfm.2025.267 Published online by Cambridge University Press

If $\theta_{1-3} = 0$, then the minimum value of T is achieved. This may be demonstrated by calculating the partial derivatives at this point. Equation (4.15) shows that the derivative by θ_{1-3} is zero. For the other two coordinates, we may choose the $\boldsymbol{k}_{1+2}$ vector. One can see from the symmetry of (2.5) that the derivatives with respect to both its components are zero.

The angular quadruplets are located further apart from the Phillips curve. The quadruplets in between are different both from DIA-like and angular ones.

4.5. *Quadruplets variety*

We have described different classes of quadruplets and the behaviour of T for these classes. Let us summarise what parts of the quadruplet manifold were studied.

The long–short interactions (characterised by $s - \sqrt{2}/2 \ll 1$) directly border the DIA-like quadruplets. In fact, the side part of the Phillips curve may be considered as the long–short interactions as it has smaller vectors of size approximately $1/4$, and larger ones of size approximately $9/4$.

The DIA-like quadruplets occupy the vicinity of the Phiilps curve ($s \approx 1$). This include the large area near the geometric singularity at the centre of the curve.

The quadruplets that are further outside the Phillips curve ($s > 1$) were not covered in the present paper. They occupy an intermediate place between the DIA-like quadruplets and the 'angular' ones, and may have properties similar to both of these kinds. The T coefficient crosses zero in this area; nevertheless, many of these quadruplets having non-zero T are significant.

The outside part of the $\boldsymbol{k}$ plane is occupied by the 'angular' quadruplets ($s \ll 1$). They have a simple asymptotic described above.

5. Conclusions

We have described the properties of the interaction coefficient T in different domains. Taken broadly, these domains cover nearly all of the quadruplet variety, with the notable exception of the quadruplets between the DIA-like and 'angular' ones.

The importance of the interaction quadruplets located at the Phillips curve, and the significance of its central zone, were shown. The behaviour of T in that domain was studied, and an explicit formula (4.2) for DIA-like quadruplets was obtained together with some approximations.

The long–short interaction asymptotics (4.12) were calculated. We have shown that both the first and second order of the T expansion in this case are zeros. Such unusual properties greatly reduce the non-locality of the kinetic equation.

We have studied the 'angular quadruplets', and we have found the minimum value -2 of the normalised T coefficient.

This study may facilitate the development of more efficient numerical models of water waves. The specific role of the singularity at the centre of the Phillips curve cannot be ignored in the models. On the other hand, the unusual smallness of the long–short interaction coefficient justifies the partial omission of such interactions. The estimates of T given above may help in testing the correctness of the models.

Funding. The author was supported by RSCF grant no. 19-72-30028 (Turbulence and coherent structures in the integrable and non-integrable systems, https://rscf.ru/en/project/19-72-30028/).

Declaration of interests. The author reports no conflict of interest.

https://doi.org/10.1017/jfm.2025.267 Published online by Cambridge University Press

Appendix A. The behaviour of T near the centre singularity

The vectors near the centre singularity are

$$\boldsymbol{k}_1 = \boldsymbol{k}_B - \varkappa_1, \quad \boldsymbol{k}_2 = \boldsymbol{k}_B + \varkappa_1, \quad \boldsymbol{k}_3 = \boldsymbol{k}_B - \varkappa_3, \quad \boldsymbol{k}_4 = \boldsymbol{k}_B + \varkappa_3, \tag{A1}$$

$$\varkappa_1 \ll k_B, \quad \varkappa_3 \ll k_B. \tag{A2}$$

We put $\boldsymbol{k}_B = \mathbf{1}$ here to simplify the formulae.

In this case,

$$s = 1 - \frac{\varkappa_{1x}^2}{8} + \frac{\varkappa_{1y}^2}{4} + o(\varkappa^2) = 1 - \frac{\varkappa_{3x}^2}{8} + \frac{\varkappa_{3y}^2}{4} + o(\varkappa^2), \tag{A3}$$

which puts the restriction on $\varkappa_1$ and $\varkappa_3$ on the resonant surface. The following formulae were derived for the resonant surface using the restriction (A3).

Equation (4.7) expanded to second order is

$$\begin{aligned} T = 2 \Bigg\{ & 1 - \frac{(\varkappa_{1x} - \varkappa_{3x})^2}{2\sqrt{(\varkappa_{1x} - \varkappa_{3x})^2 + (\varkappa_{1y} - \varkappa_{3y})^2}} \\ & - \frac{(\varkappa_{1x} + \varkappa_{3x})^2}{2\sqrt{(\varkappa_{1x} + \varkappa_{3x})^2 + (\varkappa_{1y} + \varkappa_{3y})^2}} \\ & + \frac{(\varkappa_{1x} - \varkappa_{3x})^4}{8\left((\varkappa_{1x} - \varkappa_{3x})^2 + (\varkappa_{1y} - \varkappa_{3y})^2\right)} \\ & + \frac{(\varkappa_{1x} + \varkappa_{3x})^4}{8\left((\varkappa_{1x} + \varkappa_{3x})^2 + (\varkappa_{1y} + \varkappa_{3y})^2\right)} \\ & - \frac{\varkappa_{1x}^2}{4} - \frac{\varkappa_{3x}^2}{4} - \frac{3\varkappa_{1y}^2}{4} - \frac{3\varkappa_{3y}^2}{4} + o(\varkappa^2) \Bigg\}. \end{aligned} \tag{A4}$$

The first-order correction here is non-positive, and the second is negative (unless $\varkappa_1 = \varkappa_3 = \mathbf{0}$). This proves that $T = 2$ is the maximum.

Let us discuss the derivatives of (A4). Let $\varkappa_{1y} = \pm\varkappa_{3y} = \varkappa_y$ and $\varkappa_{1y} \neq 0$, $\varkappa_{3y} \neq 0$ (this can take place on the resonant surface outside of the Phillips curve where $s > 1$). Then

$$T = 2\left(1 - \frac{1}{2}|\varkappa_{1x} \pm \varkappa_{3x}|\right) + o(\varkappa) \tag{A5}$$

and

$$\frac{\partial T}{\partial \varkappa_{1x}} = \pm 1, \quad \frac{\partial T}{\partial \varkappa_{3x}} = \pm 1 \tag{A6}$$

(the sign in (A6) depends on the sign of the corresponding $\varkappa_x$). The derivatives are non-continuous due to the presence of the terms with k_{1-3} and k_{1-4} in (2.5).

For $\varkappa_{1x} = \varkappa_{3x} = 0$, we have $\partial T/\partial \varkappa_y = 0$. For this case, we may calculate the second derivative as

$$\frac{\partial^2 T}{\partial \varkappa_y^2} = -6. \tag{A7}$$

Other derivatives do not exist due to the non-continuity of (A6).

https://doi.org/10.1017/jfm.2025.267 Published online by Cambridge University Press

We may also put $\varkappa_{1y} = \varkappa_{3y} = 0$, which corresponds to the collinear vectors (inside the Phillips curve). In this case, if we set $|\varkappa_{1x}| > |\varkappa_{3x}|$, then

$$T = 2\,(1 - |\varkappa_{1x}|) + o(\varkappa). \tag{A8}$$

Appendix B. Calculation of T for long–short interactions

B.1. *A simpler form of T*

We base our calculation on the form of T proposed in Geogjaev & Zakharov (2017):

$$\begin{aligned} T_{\boldsymbol{k}_1\boldsymbol{k}_2\boldsymbol{k}_3\boldsymbol{k}_4} = &-\frac{1}{4(k_1k_2k_3k_4)^{1/4}} \\ &+\left\{\frac{1}{2}\left(k_{1+2}^2-(\omega_1+\omega_2)^4\right)\left[(\boldsymbol{k}_1\boldsymbol{k}_2-k_1k_2)+(\boldsymbol{k}_3\boldsymbol{k}_4-k_3k_4)\right]\right. \\ &-\frac{1}{2}\left(k_{1-3}^2-(\omega_1-\omega_3)^4\right)\left[(\boldsymbol{k}_1\boldsymbol{k}_3+k_1k_3)+(\boldsymbol{k}_2\boldsymbol{k}_4+k_2k_4)\right] \\ &-\frac{1}{2}\left(k_{1-4}^2-(\omega_1-\omega_4)^4\right)\left[(\boldsymbol{k}_1\boldsymbol{k}_4+k_1k_4)+(\boldsymbol{k}_2\boldsymbol{k}_3+k_2k_3)\right] \\ &+\left(\frac{4(\omega_1+\omega_2)^2}{k_{1+2}-(\omega_1+\omega_2)^2}-1\right)(\boldsymbol{k}_1\boldsymbol{k}_2-k_1k_2)(\boldsymbol{k}_3\boldsymbol{k}_4-k_3k_4) \\ &+\left(\frac{4(\omega_1-\omega_3)^2}{k_{1-3}-(\omega_1-\omega_3)^2}-1\right)(\boldsymbol{k}_1\boldsymbol{k}_3+k_1k_3)(\boldsymbol{k}_2\boldsymbol{k}_4+k_2k_4) \\ &\left.+\left(\frac{4(\omega_1-\omega_4)^2}{k_{1-4}-(\omega_1-\omega_4)^2}-1\right)(\boldsymbol{k}_1\boldsymbol{k}_4+k_1k_4)(\boldsymbol{k}_2\boldsymbol{k}_3+k_2k_3)\right\}. \end{aligned} \tag{B1}$$

This form is equivalent to (2.5) on the resonant surface (but differs outside it). Here, we have set $g = 1$.

The transition from (2.5) to (B1) is done with the use of the following identities. First,

$$\begin{aligned} (\boldsymbol{k}_1\boldsymbol{k}_2+k_1k_2)(\boldsymbol{k}_3\boldsymbol{k}_4+k_3k_4)-4k_1k_2k_3k_4 = &(\boldsymbol{k}_1\boldsymbol{k}_2-k_1k_2)(\boldsymbol{k}_3\boldsymbol{k}_4-k_3k_4) \\ &+2k_3k_4(\boldsymbol{k}_1\boldsymbol{k}_2-k_1k_2)+2k_1k_2(\boldsymbol{k}_3\boldsymbol{k}_4-k_3k_4) \end{aligned} \tag{B2}$$

and its analogues for two other similar terms in (2.5). Second,

$$\begin{aligned} k_{1+2}^2-(\omega_1+\omega_2)^4 &= 2(\boldsymbol{k}_1\boldsymbol{k}_2-k_1k_2)-4\omega_1\omega_2(\omega_1+\omega_2)^2-4k_1k_2 \\ &= 2(\boldsymbol{k}_3\boldsymbol{k}_4-k_3k_4)-4\omega_3\omega_4(\omega_3+\omega_4)^2-4k_3k_3 \end{aligned} \tag{B3}$$

and its analogues. (Here, the resonance condition (2.3) is used.)

B.2. *The asymptotic of T*

In this subsection, we calculate the asymptotic (4.12). We take T of the form (B1) for this calculation.

We use the parameter r such that

$$\omega_1+\omega_2 = \omega_3+\omega_4 = (1+r)\sqrt{gk_{1+2}}. \tag{B4}$$

This parameter may generally be used instead of s ($r = \sqrt{2}\,s - 1$). For the long–short interactions, we have $\omega_1 \ll \omega_2$ and $\omega_3 \ll \omega_4$, and r becomes a small parameter: $r \ll 1$.

https://doi.org/10.1017/jfm.2025.267 Published online by Cambridge University Press

The other independent variables that we will use are p_1 and p_3 such that

$$\omega_1\omega_2 = k_{1+2}\, r\, \left(1+\frac{rp_1}{2}\right), \quad \omega_3\omega_4 = k_{1+2}\, r\, \left(1+\frac{rp_3}{2}\right). \tag{B5}$$

We will show that

$$p_1 \approx \cos\theta_1, \quad p_3 \approx \cos\theta_3, \tag{B6}$$

where θ_1 is an angle between $\boldsymbol{k}_1$ and $\boldsymbol{k}_{1+2}$, and θ_3 is an angle between $\boldsymbol{k}_3$ and $\boldsymbol{k}_{1+2}$. The calculation below is based on p_1 and p_3 variables, and does not use the angles directly.

The variables introduced allow direct calculation of ω_i. For our purpose, the following expansion by r is sufficient:

$$\begin{aligned}
\omega_1 &= \sqrt{k_{1+2}}\left(r+\frac{r^2p_1}{2}+\frac{r^3p_1}{2}+o\big(r^3\big)\right), \quad \omega_2 = \sqrt{k_{1+2}}\left(1-\frac{r^2p_1}{2}-\frac{r^3p_1}{2}+o\big(r^3\big)\right),\\
\omega_3 &= \sqrt{k_{1+2}}\left(r+\frac{r^2p_3}{2}+\frac{r^3p_3}{2}+o\big(r^3\big)\right), \quad \omega_4 = \sqrt{k_{1+2}}\left(1-\frac{r^2p_3}{2}-\frac{r^3p_3}{2}+o\big(r^3\big)\right).
\end{aligned} \tag{B7}$$

Note that $\omega_1-\omega_3 = O(r^2)$. This difference is smaller than both ω_1 and ω_3.

We will use k_{1+2} as the quadruplet norm, and set $k_{1+2}=1$ to simplify the formulae.

We begin with the calculation of the fractions in (B1):

$$\begin{aligned}
&\frac{4(\omega_1+\omega_2)^2}{k_{1+2}-(\omega_1+\omega_2)^2}-1 = -\left(2r^{-1}+4+\frac{r}{2}+o(r)\right),\\
&\frac{4(\omega_1-\omega_3)^2}{k_{1-3}-(\omega_1-\omega_3)^2}-1 = -1+o(r),\\
&\frac{4(\omega_1-\omega_4)^2}{k_{1-4}-(\omega_1-\omega_4)^2}-1 = 2r^{-1}-4+\frac{r}{2}-r(p_1+p_3)+o(r).
\end{aligned} \tag{B8}$$

To calculate the third fraction, we have used the following expression for k_{1-4}:

$$k_{1-4}^2 = k_{1+2}^2\big(1-2r^2(p_1+p_3)-2r^3(p_1+p_3)\big)+o\big(r^3\big). \tag{B9}$$

Let us note that

$$\begin{aligned}
&(\boldsymbol{k}_1\boldsymbol{k}_4+k_1k_4)+(\boldsymbol{k}_2\boldsymbol{k}_3+k_2k_3) = r^2(p_1+p_3+2)+o\big(r^2\big),\\
&(\boldsymbol{k}_1\boldsymbol{k}_4+k_1k_4)(\boldsymbol{k}_2\boldsymbol{k}_3+k_2k_3) = r^4(p_1+1)(p_3+1)+o\big(r^4\big).
\end{aligned} \tag{B10}$$

Now (B1) takes the form

$$\begin{aligned}
T_{\boldsymbol{k}_1\boldsymbol{k}_2\boldsymbol{k}_3\boldsymbol{k}_4} = \frac{1}{4r}\Big\{&\left(2r+2r^3\right)\, S_1+3r^2D_1+4S_2+\left(2r^{-1}+\frac{r}{2}\right)\, D_2\\
&+4r^4+r^5\Big((p_1+p_3)p_1p_3-2(p_1+p_3)^2-(p_1+p_3)\Big)+o\big(r^5\big)\Big\},
\end{aligned} \tag{B11}$$

where

$$\begin{aligned}
S_1 &= [(\boldsymbol{k}_1\boldsymbol{k}_2-k_1k_2)+(\boldsymbol{k}_3\boldsymbol{k}_4-k_3k_4)]+[(\boldsymbol{k}_1\boldsymbol{k}_4+k_1k_4)+(\boldsymbol{k}_2\boldsymbol{k}_3+k_2k_3)],\\
D_1 &= [(\boldsymbol{k}_1\boldsymbol{k}_2-k_1k_2)+(\boldsymbol{k}_3\boldsymbol{k}_4-k_3k_4)]-[(\boldsymbol{k}_1\boldsymbol{k}_4+k_1k_4)+(\boldsymbol{k}_2\boldsymbol{k}_3+k_2k_3)],\\
S_2 &= (\boldsymbol{k}_1\boldsymbol{k}_2-k_1k_2)(\boldsymbol{k}_3\boldsymbol{k}_4-k_3k_4)+(\boldsymbol{k}_1\boldsymbol{k}_4+k_1k_4)(\boldsymbol{k}_2\boldsymbol{k}_3+k_2k_3),\\
D_2 &= (\boldsymbol{k}_1\boldsymbol{k}_2-k_1k_2)(\boldsymbol{k}_3\boldsymbol{k}_4-k_3k_4)-(\boldsymbol{k}_1\boldsymbol{k}_4+k_1k_4)(\boldsymbol{k}_2\boldsymbol{k}_3+k_2k_3).
\end{aligned} \tag{B12}$$

https://doi.org/10.1017/jfm.2025.267 Published online by Cambridge University Press

Our variables allow for the exact expressions for the scalar products

$$\boldsymbol{k}_1\boldsymbol{k}_2 = r^2 p_1 + r^3 p_1 + r^4\left(-\frac{1}{2} + p_1 - \frac{p_1^2}{4}\right),$$
$$\boldsymbol{k}_3\boldsymbol{k}_4 = r^2 p_3 + r^3 p_3 + r^4\left(-\frac{1}{2} + p_3 - \frac{p_3^2}{4}\right). \tag{B13}$$

(This was obtained by squaring the expression $\boldsymbol{k}_{1+2} = \boldsymbol{k}_1 + \boldsymbol{k}_2$ (and its analogue) and using (B5) and (B4).)

The expression (B13) results in (B6).

The scalar product $\boldsymbol{k}_1\boldsymbol{k}_4$ may be calculated with the use of the relation $\boldsymbol{k}_4 = \boldsymbol{k}_2 + \boldsymbol{k}_1 - \boldsymbol{k}_3$:

$$\boldsymbol{k}_1\boldsymbol{k}_4 = \boldsymbol{k}_1\boldsymbol{k}_2 + k_1^2 - \boldsymbol{k}_1\boldsymbol{k}_3. \tag{B14}$$

In the same way,

$$\boldsymbol{k}_3\boldsymbol{k}_2 = \boldsymbol{k}_3\boldsymbol{k}_4 + k_3^2 - \boldsymbol{k}_1\boldsymbol{k}_3. \tag{B15}$$

The last two terms here are of order $O(r^4)$. We have

$$\boldsymbol{k}_1\boldsymbol{k}_4 = \boldsymbol{k}_1\boldsymbol{k}_2 + O\left(r^4\right), \quad \boldsymbol{k}_3\boldsymbol{k}_2 = \boldsymbol{k}_3\boldsymbol{k}_4 + O\left(r^4\right). \tag{B16}$$

We will also need the following:

$$k_1k_2 = r^2\left(1 + rp_1 + \frac{r^2p_1^2}{4}\right),$$
$$k_3k_4 = r^2\left(1 + rp_3 + \frac{r^2p_3^2}{4}\right),$$
$$k_1k_4 = r^2\left(1 + rp_1 + \frac{r^2p_1^2}{4} + r^2(p_1 - p_3) + o\left(r^2\right)\right),$$
$$k_3k_2 = r^2\left(1 + rp_3 + \frac{r^2p_3^2}{4} + r^2(p_3 - p_1) + o\left(r^2\right)\right). \tag{B17}$$

Finally, we note that

$$\boldsymbol{k}_2 - \boldsymbol{k}_4 = \boldsymbol{k}_3 - \boldsymbol{k}_1 = O\left(r^2\right). \tag{B18}$$

The calculation results in

$$S_1 = (\boldsymbol{k}_1 + \boldsymbol{k}_3)\,(\boldsymbol{k}_2 + \boldsymbol{k}_4) + o\left(r^4\right), \tag{B19}$$

$$D_1 = -4r^2 - 2r^3(p_1 + p_3) + o\left(r^3\right), \tag{B20}$$

$$S_2 = r^4\left(2 + 2p_1p_3\right) + r^5\left(2(p_1 + p_3) + 4rp_1p_3\right) + o\left(r^5\right). \tag{B21}$$

https://doi.org/10.1017/jfm.2025.267 Published online by Cambridge University Press

The calculation of D_2 is the most complex; it requires three orders of precision. The result is

$$D_2 = -r^2\,(\boldsymbol{k}_1+\boldsymbol{k}_3)\,(\boldsymbol{k}_2+\boldsymbol{k}_4) - 4r^5 p_1 p_3 + r^2(p_1+p_3)\boldsymbol{k}_1\boldsymbol{k}_3 - r^6(p_1+p_3) + r^6\left(-4p_1p_3 - \frac{p_1p_3}{2}(p_1+p_3) + (p_1-p_3)(p_1-p_3)\right) + o\big(r^6\big). \tag{B22}$$

The summation yields

$$T = \frac{r^4 k_{1+2}^3}{2}\left\{2r^5(p_1+p_3) + 2r(p_1+p_3)\boldsymbol{k}_1\boldsymbol{k}_3\right\}. \tag{B23}$$

Then, substituting $\boldsymbol{k}_1\boldsymbol{k}_3 = r^4\cos(\theta_1-\theta_3) + o(r^4)$ and using (B6), we get the final result in (4.12):

$$T = \frac{r^4 k_{1+2}^3}{2}\,(\cos\theta_1+\cos\theta_3)\,(1+\cos(\theta_1-\theta_3)) + o\big(r^4\big). \tag{B24}$$

References

Alves, J.-H., *et al.* 2007 Wave modelling – the state of the art. *Prog. Oceanogr.* **75** (4), 603–674.

Annenkov, S.Yu & Shrira, V.I. 2001 Numerical modelling of water-wave evolution based on the Zakharov equation. *J. Fluid Mech.* **449**, 341–371.

Annenkov, S.Yu & Shrira, V.I. 2013 Large-time evolution of statistical moments of wind-wave fields. *J. Fluid Mech.* **726**, 517–546.

Badulin, S.I., Pushkarev, A.N., Resio, D. & Zakharov, V.E. 2005 Self-similarity of wind-driven seas. *Nonlinear Process. Geophys.* **12** (6), 891–945.

Benoit, M. 2005 Evaluation of methods to compute the non-linear quadruplet interactions for deep-water wave spectra. In 5th International Symposium on Ocean Wave Measurement and Analysis (WAVES'2005), 52, ASCE , Madrid, Spain, pp 1–10.

Dungey, J.C. & Hui, W.H. 1979 Nonlinear energy transfer in a narrow gravity-wave spectrum, *Proc. R. Soc. Lond. A: Math. Phys. Sci.* **368**. 239–265.

Dyachenko, A.I., Kachulin, D.I. & Zakharov, V.E. 2017 Super compact equation for water waves. *J. Fluid Mech.* **828**, 661–679.

Dyachenko, A.I. & Zakharov, V.E. 1994 Is free-surface hydrodynamics an integrable system? *Phys. Lett. A* **190** (2), 144–148.

Dysthe, K.B. 1979 Note on a modification to the nonlinear Schrödinger equation for application to deep water waves. *Proc. R. Soc. Lond. A: Math. Phys. Sci.* **369**, 105–114.

Gagnaire-Renou, E., Benoit, M. & Badulin, S.I. 2011 On weakly turbulent scaling of wind sea in simulations of fetch-limited growth. *J. Fluid Mech.* **669**, 178–213.

Geogjaev, V.V. & Zakharov, V.E. 2017 Numerical and analytical calculations of the parameters of power-law spectra for deep water gravity waves. *J. Expl Theor. Phys. Lett.* **106** (3), 184–187.

Hashimoto, N. & Kawaguchi, K. 2001 Extension and modification of discrete interaction approximation (DIA) for computing nonlinear energy transfer of gravity wave spectra. In Fourth International Symposium on Ocean Wave Measurement and Analysis, Proceedings, "American Society of Civil Engineers", vol. **1**, pp. 530–539.

Hasselmann, K. 1962 On the non-linear energy transfer in a gravity-wave spectrum. Part 1. General theory. *J. Fluid Mech.* **12**, 481–500.

Hasselmann, S., Hasselmann, K., Allender, J.H. & Barnett, T.P. 1985 Computations and parameterizations of the nonlinear energy transfer in a gravity-wave specturm. Part II: Parameterizations of the nonlinear energy transfer for application in wave models. *J. Phys. Oceanogr.* **15** (11), 1378–1391.

Komen, G.J., Cavaleri, L., Donelan, M., Hasselmann, K., Hasselmann, S. & Janssen, P.A.E.M. 1994 *Dynamics and Modelling of Ocean Waves*. Cambridge University Press, section 'III.3.2 Nonlinear transfer'.

Komen, G.J., Hasselmann, S. & Hasselmann, K. 1984 On the existence of a fully developed wind–sea spectrum. *J. Phys. Oceanogr.* **14** (8), 1271–1285.

Krasitskii, V.P. 1994 On reduced equations in the Hamiltonian theory of weakly nonlinear surface waves. *J. Fluid Mech.* **272**, 1–20.

https://doi.org/10.1017/jfm.2025.267 Published online by Cambridge University Press

LAVRENOV, I.V. 2003 *Wind-Waves in Oceans: Dynamics and Numerical Simulations*. Springer Science & Business Media, 2003.

LAVROVA, O.YU 1983 On the lateral instability of waves on the surface of a finite-depth fluid. *Izv. Atmos. Ocean. Phys.* **19** (10), 807–810.

LONGUET-HIGGINS, M.S. 1976 On the nonlinear transfer of energy in the peak of a gravity-wave spectrum: a simplified model. *Proc. R. Soc. Lond. A* **347**, 311–328.

PHILLIPS, O.M. 1960 On the dynamics of unsteady gravity waves of finite amplitude. *J. Fluid Mech.* **9** (2), 193–217.

TOLMAN, H.L. 2004 Inverse modeling of discrete interaction approximations for nonlinear interactions in wind waves. *Ocean Model.* **6** (3–4), 405–422.

WEBB, D.J. 1978 Non-linear transfers between sea waves. *Deep Sea Res.* **25** (3), 279–298.

ZAKHAROV, V.E. 1968 Stability of periodic waves of finite amplitude on the surface of a deep fluid. *J. Appl. Mech. Tech. Phys.* **9** (2), 190–194.

ZAKHAROV, V.E. 1999 Statistical theory of gravity and capillary waves on the surface of a finite-depth fluid. *Eur. J. Mech. B/Fluids* **18** (3), 327–344.

ZAKHAROV, V.E., BADULIN, S.I., GEOGJAEV, V.V. & PUSHKAREV, A.N. 2019 Weak-turbulent theory of wind-driven sea. *Earth Space Sci.* **6** (4), 540–556.

ZAKHAROV, V.E. & FILONENKO, N.N. 1966 Energy spectrum for stochastic oscillations of the surface of liquid. *Dokl. Acad. Nauk SSSR* **1960**, 1292–1295.

https://doi.org/10.1017/jfm.2025.267 Published online by Cambridge University Press